nature physics

Article

https://doi.org/10.1038/s41567-023-02248-4

Mediated interactions between Fermi polarons and the role of impurity quantum statistics

Received: 8 May 2023

Accepted: 14 September 2023

Published online: 26 October 2023

Check for updates

Cosetta Baroni[1,2] ✉, Bo Huang[1,2], Isabella Fritsche[1,2], Erich Dobler[1,2], Gregor Anich[1,2], Emil Kirilov[1,2], Rudolf Grimm[1,2], Miguel A. Bastarrachea-Magnani[3], Pietro Massignan[4] & Georg M. Bruun[5]

The notion of quasi-particles is essential for understanding the behaviour of complex many-body systems. A prototypical example of a quasi-particle is a polaron, formed by an impurity strongly interacting with a surrounding medium. Fermi polarons, created in a Fermi sea, provide a paradigmatic realization of this concept. Importantly, such quasi-particles interact with each other via the modulation of the medium. However, although quantum simulation experiments with ultracold atoms have substantially improved our understanding of individual polarons, the detection of their interactions has so far remained elusive. Here we report the observation of mediated interactions between Fermi polarons consisting of K impurities embedded in a Fermi sea of Li atoms. Our results confirm two predictions of Landau's Fermi-liquid theory: the shift in polaron energy due to mediated interactions, which is linear in the concentration of impurities; and its sign inversion with impurity quantum statistics. For weak-to-moderate interactions between the impurities and the medium, our results agree with the static predictions of Fermi-liquid theory. For stronger impurity–medium interactions, we show that the observed behaviour at negative energies can be explained by a more refined many-body treatment including retardation and dressed molecule formation.

The theory of Fermi liquids, introduced by Landau in the late 1950s, lies at the heart of our understanding of quantum many-body systems such as atomic nuclei, liquid helium-3, electrons in solid-state materials, Kondo impurities and neutron stars[1,2]. Landau's key intuition was to explain the behaviour of many complex many-body systems in terms of elementary excitations dubbed quasi-particles. The strong interactions between the fundamental constituents may be absorbed into few parameters characterizing the quasi-particles, such as their energy and effective mass. This allows for a dramatically simplified description akin to that of the weakly interacting particles.

An inherent property of quasi-particles is that they mutually interact by modulating the surrounding medium. For instance, phonon-mediated interactions give rise to conventional superconductivity, whereas spin waves are conjectured to mediate the interactions that lead to high-temperature superconductivity. The interaction between quasi-particles due to the exchange of particle–hole excitations in a surrounding Fermi sea (FS) is crucial for understanding

[1]Institut für Quantenoptik und Quanteninformation (IQOQI), Österreichische Akademie der Wissenschaften, Innsbruck, Austria. [2]Institut für Experimentalphysik, Universität Innsbruck, Innsbruck, Austria. [3]Departamento de Física, Universidad Autónoma Metropolitana-Iztapalapa, Ciudad de México, Mexico. [4]Departament de Física, Universitat Politècnica de Catalunya, Barcelona, Spain. [5]Department of Physics and Astronomy, Aarhus University, Aarhus, Denmark. ✉e-mail: cosetta.baroni@uibk.ac.at

both equilibrium and dynamical properties of Fermi liquids. This is of particular importance for the emergence of collective modes in Fermi liquids[2] and the appearance of giant magneto-resistance, as well as for the coupling between nuclear magnetic moments as predicted by Ruderman, Kittel, Kasuya and Yosida[1].

The experimental approach of quantum simulation with ultracold atoms has substantially improved our understanding of single quasi-particles. Here the quasi-particle is formed by an impurity atom surrounded by a Fermi gas or a Bose–Einstein condensate (BEC)[3–7] and is referred to as a Fermi polaron or Bose polaron, respectively. In a recent experiment[8], fermion-mediated interactions between atoms in a BEC were observed under conditions of rather weak interspecies interaction. In the strongly interacting regime, interferometric spectroscopy in the time domain[9] revealed a loss of contrast in the case of a non-zero impurity concentration, but an unambiguous detection of the quasi-particle interaction in the strongly interacting regime has remained elusive[3,7]. Experiments on out-of-equilibrium two-dimensional materials demonstrated interactions between excitons mediated by electrons, but with a sign opposite to the one predicted by Fermi-liquid theory for a system in equilibrium[10,11].

In this work, we report on the observation of mediated interactions between Fermi polarons formed by either bosonic ^{41}K or fermionic ^{40}K atoms in a FS of ^{6}Li atoms. By choosing the K isotope, our system offers the unique possibility to change the impurity quantum statistics, leaving everything else essentially unchanged. From the observed linear shift in the polaron energy with increasing concentration, we extract a momentum-averaged quasi-particle interaction. Taking advantage of the exceptional degrees of control offered by the ultracold quantum gas mixture, we examine this interaction as a function of the sign and strength of the K–Li interaction and find excellent agreement with the predictions of Fermi-liquid theory for weak-to-moderate interaction strengths. This includes a predicted sign reversal of the mediated quasi-particle interaction with the impurity quantum statistics. For strong interactions, we observe deviations from Landau theory, which may be explained by the disappearance of the polaron and the emergence of molecular excitations on the attractive side.

Within Fermi-liquid theory, an impurity (↓) interacting with a degenerate FS of (↑) particles forms a quasi-particle. The energy of such a Fermi polaron depends on the strength of the interaction between the impurity and the particles in the FS, which—for a short-range interaction—can be characterized by the dimensionless parameter $X = -1/(k_F a)$. Here a is the s-wave interspecies scattering length and $k_F = (6\pi^2 n_\uparrow)^{1/3} = \sqrt{2m_\uparrow \epsilon_F}/\hbar$ is the Fermi wave number, with $m_\uparrow$ being the mass of particles forming the FS; $n_\uparrow$, their number density; ϵ_F, the Fermi energy of the FS; and $\hbar$, the reduced Planck constant. The energy $\epsilon^0_{\mathbf{k}\downarrow}$ of a single polaron with momentum $\mathbf{k}$ and mass $m_\downarrow$ is then, for a given mass ratio $m_\downarrow/m_\uparrow$, a universal function of X (refs. 12–19), which has been widely studied in previous experiments[3,4,7,20,21].

By increasing the concentration of impurities, that is, $\mathcal{C} = n_\downarrow/n_\uparrow$, more polarons are formed, and they interact with each other via density modulations in the medium. According to Landau's theory, the energy needed for creating a polaron with momentum $\mathbf{k}$ can, for small $\mathcal{C}$, be written as[2]

$$\epsilon_{\mathbf{k}\downarrow} = \epsilon^0_{\mathbf{k}\downarrow} + \sum_{\mathbf{k}'} f_{\mathbf{k},\mathbf{k}'} n_{\mathbf{k}'\downarrow}, \quad (1)$$

where $f_{\mathbf{k},\mathbf{k}'}$ represents the interaction between two polarons with momenta $\mathbf{k}$ and $\mathbf{k}'$ mediated by atoms of the medium, and $n_{\mathbf{k}\downarrow}$ is the momentum-resolved polaron density. One can calculate the quasi-particle interaction to the second order in the polaron–medium interaction $\partial\epsilon_F/\partial n_\downarrow$, where $n_\downarrow = \sum_{\mathbf{k}} n_{\mathbf{k}\downarrow}$ is the total impurity density[22–24]. In the limit of vanishing energy and momenta, this yields

$$f_0 = \mp \frac{2\epsilon_F}{3n_\uparrow}(\Delta N)^2, \quad (2)$$

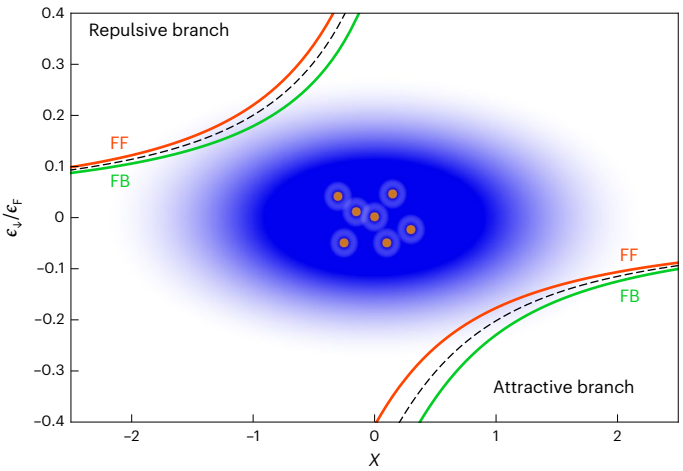

Fig. 1 | Polaron energy including mediated interactions. The energy of attractive and repulsive polarons is presented as a function of the dimensionless interaction parameter X according to equation (3) using the static limit for the polaron–polaron-mediated interaction defined in equation (2). The results are shown for the limit of a single impurity (that is, $\mathcal{C} = 0$; black dashed lines) and for impurity concentration $\mathcal{C} = 0.5$ in FB (solid green lines) and FF (solid red lines) K–Li mixtures.

where $\Delta N = -\partial\epsilon^0_{0\downarrow}/\partial\epsilon_F$ is the number of particles in the dressing cloud around a zero-momentum impurity[25]. Equation (2), which—in the perturbative regime—can be microscopically derived using many-body theory (Supplementary Section II), demonstrates that the sign of the induced interaction explicitly depends on the quantum statistics of the impurities.

To facilitate comparison with our spectroscopy experiment, which is not momentum resolved, we average equation (1) over momentum and write

$$\epsilon_\downarrow = \epsilon^0_\downarrow + \bar{f} n_\uparrow \mathcal{C}, \quad (3)$$

where $\bar{f} = \sum_{\mathbf{k}\mathbf{k}'} n_{\mathbf{k}\downarrow} f_{\mathbf{k},\mathbf{k}'} n_{\mathbf{k}'\downarrow}/n^2_\downarrow$ represents the average of the quasi-particle interaction $f_{\mathbf{k},\mathbf{k}'}$. We introduce the dimensionless quantity $\bar{f} n_\uparrow/\epsilon_F$ and, in the following, we refer to it as the mediated interaction coefficient. In equation (3), we neglect the direct interaction between the bare impurities, since the latter is negligible in our experiment (Methods).

In Fig. 1, we illustrate the interaction dependence of the attractive and repulsive polaron energies according to equation (3), with $\bar{f} = f_0$ given by equation (2), for three example cases: single impurity (dashed black lines) and for a finite concentration for bosonic (green solid lines) and fermionic (red solid lines) impurities. This figure also highlights that the mediated interaction effect (exaggerated by choosing a large concentration $\mathcal{C} = 0.5$) is rather weak, which makes its observation very challenging in an actual experiment.

The main motivation of our experimental work is to use the unique level of control offered by atomic quantum gases to systematically explore the interaction between quasi-particles. This includes testing the behaviour of the sign of the mediated interaction, which is predicted to be independent of the attractive or repulsive character of the impurity–medium interaction, but which should undergo a sign reversal with the impurity quantum statistics. More generally, we will test the validity of Landau's quasi-particle theory for increasing the impurity concentration and variable interaction strengths.

Our experiments are carried out with a mixed-species system, which consists of a trapped spin-polarized FS of ^{6}Li atoms in which either bosonic or fermionic impurity atoms are immersed (^{41}K or ^{40}K).

https://doi.org/10.1038/s41567-023-02248-4

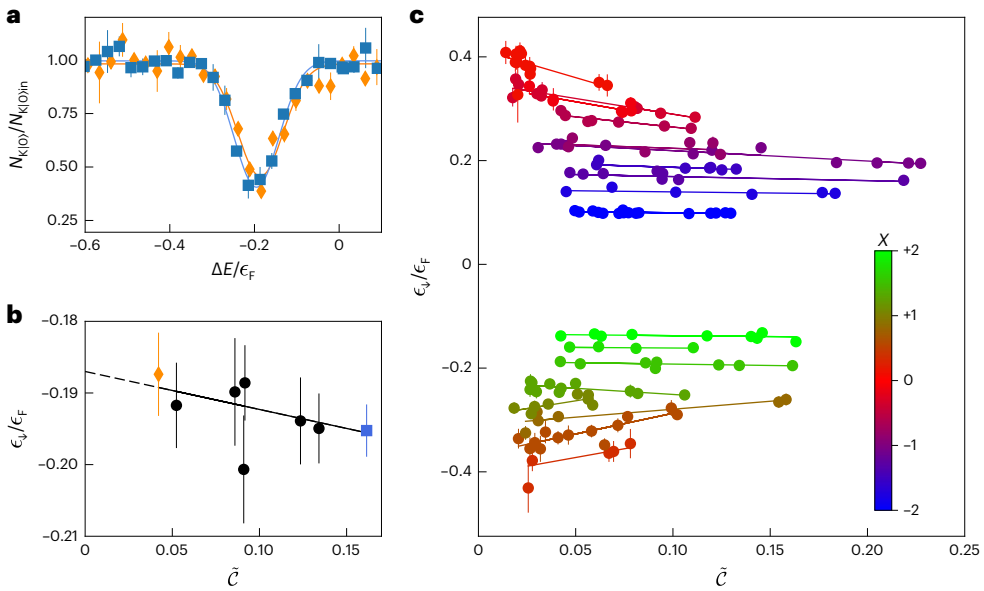

Fig. 2 | Dependence of polaron energy on the impurity concentration. For the FB case, the main steps of measurements and data analysis are illustrated. **a**, Two example spectroscopy signals (normalized to the initial atom number) taken at $X = 0.98$ for different values of the interacting impurity concentration (blue squares, $\tilde{C} = 0.16$; orange diamonds, $\tilde{C} = 0.04$). The solid lines are fits with a Gaussian function on a linear background (the latter being negligibly small in the present data). The error bars represent the standard errors from typically 5–6 measurement repetitions. **b**, Polaron energy as a function of impurity concentration for $X = 0.98$. The blue square and the orange diamond correspond to the example spectra presented in **a**. The black line represents a linear fit to the data, with the dashed line showing the extrapolation to zero density. **c**, Polaron energy as a function of impurity concentration for different values of interaction parameter X. From centre to top (blue to red), increasing repulsion; from centre to bottom (green to red), increasing attraction. Statistical uncertainties in **b** and **c** are evaluated taking into account the fit uncertainties from analysing the spectra and errors on the Fermi energy.

The possibility to change the impurity statistics from bosonic to fermionic, and keeping all the other features nearly identical, is a key feature of our system, allowing for a direct observation of the effect of the impurity statistics in the polaron problem. Moreover, we benefit from the K–Li mass imbalance ($m_\downarrow/m_\uparrow \approx 6.8$) in several ways. First, it allows to prepare a system with a high impurity concentration where the fermionic medium is deeply degenerate as the impurities remain in the thermal regime (Supplementary Fig. 1). This avoids complications arising for degenerate impurities, such as energy shifts resulting from Pauli blocking for fermionic impurities[3,7,26], or phase separation or collapse when a BEC of bosonic impurities is formed[21]. Moreover, the thermal energy distribution of impurities is insensitive to the difference between their bare and effective mass, the effects of which can—in the degenerate regime—dominate over mediated interactions[7] (Supplementary Fig. 1).

As a further benefit, the strong Fermi pressure of the lighter atoms of the medium results in a spatial extent of the FS that is large compared with the cloud size of the heavier impurity atoms. This effect (further enhanced by the tighter optical trapping potential for K in near-infrared light[4]) leads to the favourable situation that the impurities in the FS experience a nearly homogeneous medium with an essentially constant chemical potential.

The basic idea of our probing method, which has been introduced in previous work[4,21], is an injection scheme based on the radio-frequency (RF) transfer from an impurity spin state $K|0\rangle$ to a state $K|1\rangle$. The initial state $K|0\rangle$ is essentially non-interacting with the medium. The target state $K|1\rangle$, instead, features tunability of the s-wave interaction with the fermionic medium via a magnetically controlled interspecies Feshbach resonance (FR) (Methods). In both mixtures (Fermi–Bose (FB) and Fermi–Fermi (FF)), a direct interaction between the impurities is negligible since the intraspecies s-wave scattering is off-resonant for bosonic ^{41}K and absent for fermionic ^{40}K (Methods). We note that in real experiments, the normalized single-polaron energy $\epsilon_\downarrow^0/\epsilon_F$ and the mediated interaction coefficient $\tilde{f}n_\uparrow/\epsilon_F$ depend not only on the parameter X but also on the mass ratio and an additional 'range parameter' (Methods), which is related to the resonance width[27,28] and, in our case, is small enough to stay in the near-universal regime. Since in the two mixtures used in our experiment, the values of these parameters are almost identical, the differences in mass ratio and FR width have a minor effect; therefore, the impurity quantum statistics is the essential difference.

The starting point of our experiments is a mixture of roughly 10^5 atoms of ^{6}Li and 10^4 atoms of ^{41}K or ^{40}K. Although the Li atoms are always kept in the lowest hyperfine spin state, the K atoms are initially prepared in a weakly interacting auxiliary state, $K|\mathrm{aux}\rangle$, from which a fraction of atoms is RF transferred to $K|0\rangle$ to vary the impurity concentration (Methods). The atoms are trapped in a 1,064 nm crossed-beam optical dipole trap in the presence of a magnetic field close to the FR. The two species are in thermal equilibrium. Although the Li FS is degenerate, the K impurities remain in the thermal regime.

To take the residual inhomogeneity of our system into account, we introduce effective quantities defined by averaging over the spatial extent of the K cloud. In particular, we introduce the K-averaged atom number densities, namely, $\bar{n}_{Li}$ and $\bar{n}_K$, for the two species, and the effective Fermi energy ϵ_F of the Li FS (Methods). These quantities and the temperature T of the sample are obtained from separate measurements performed before each main polaron measurement. Typical values of the effective Li density, effective Fermi energy and reduced temperature are similar for the two mixtures. In particular we have $\bar{n}_{Li} \approx 1.5 \times 10^{12}$ cm^{-3}, $\epsilon_F/h \approx 16$ kHz and $T/T_F \approx 0.15$ for the FB mixture and $\bar{n}_{Li} \approx 2.0 \times 10^{12}$ cm^{-3}, $\epsilon_F/h \approx 20$ kHz and $T/T_F \approx 0.25$ for the FF mixture.

We implement the RF spectroscopic probing scheme by applying a 1 ms Blackman-shaped pulse. The pulse duration is chosen as a compromise between the spectral width of the RF pulse ($\sigma_{RF} \approx 0.7$ kHz) and the shortest polaron lifetime (of the order of a few milliseconds for strong repulsion[4,21]). The pulse intensity is adjusted to obtain a resonant π-pulse in the absence of Li atoms. We vary the pulse frequency ν

https://doi.org/10.1038/s41567-023-02248-4

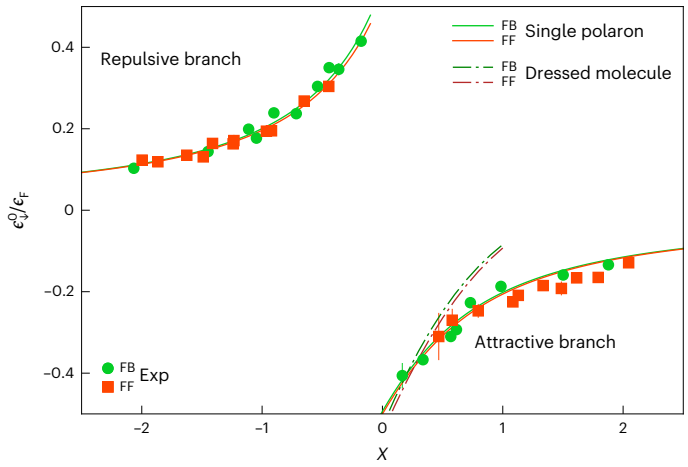

Fig. 3 | Polaron energy in the single-impurity limit. The experimental results for $\epsilon_\downarrow^0/\epsilon_F$ for the FB (green circles) and FF (red squares) mixtures are compared with the theoretically expected values for a single polaron (green and red solid lines for FB and FF, respectively). In addition, we show the energy of the dressed molecules (green and red dash–dot lines for FB and FF, respectively). Note that the theory lines are almost identical for the FB and FF cases; therefore, they overlap to a large extent. The error bars for $\epsilon_\downarrow^0/\epsilon_F$ correspond to the uncertainties of the linear fit and the errors on the Fermi energy. The error bars for X, smaller than the symbol size, represent the standard errors for each set of measurements.

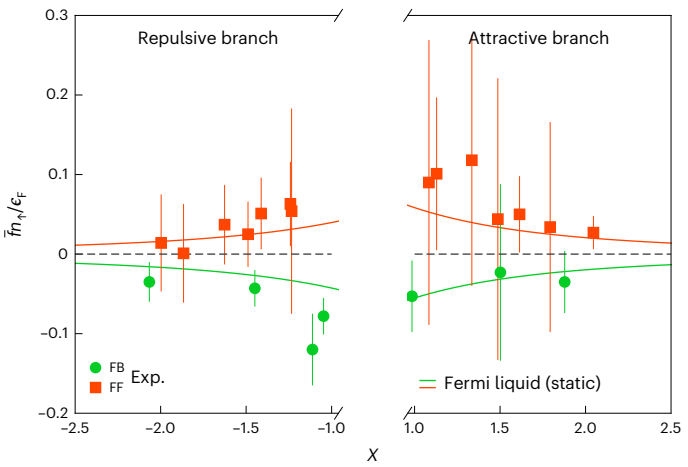

Fig. 4 | Mediated interaction coefficient in the regime of moderate impurity–medium interactions. The experimental results for $\bar{f}n_\uparrow/\epsilon_F$ for FB (green circles) and FF (red squares) are compared with equation (3), with $\bar{f}$ given by the static limit of the Fermi-liquid theory of equation (2) (green and red solid lines refer to FB and FF cases, respectively) for interaction values of $|X| \gtrsim 1$. The plot refers to the repulsive and attractive branches for negative and positive values of X, respectively. The error bars on $\bar{f}n_\uparrow/\epsilon_F$ correspond to the uncertainties of the linear fit and the errors on the Fermi energy. The error bars on X, smaller than the symbol size, represent the standard errors for each set of measurements.

to probe the polaron spectrum. Our spectroscopic observable is the number $N_{K|0\rangle}$ of atoms remaining in $K|0\rangle$ after the RF pulse (Methods). We define the detuning $\Delta E = h(\nu_0 - \nu)$ for the FB case and $\Delta E = h(\nu - \nu_0)$ for the FF case, where ν_0 is the bare frequency of the $K|0\rangle$ to $K|1\rangle$ transition in the absence of Li. The opposite sign in the definitions of ΔE takes into account the fact that in our FB mixture, $K|0\rangle$ has a higher energy than $K|1\rangle$ and vice versa in our FF mixture. For both cases, the polaron spectrum is then represented by $N_{K|0\rangle}(\Delta E/\varepsilon_F)$.

In Fig. 2a, we show a typical RF transfer signal, recorded for bosonic ^{41}K impurities, for two different impurity concentrations. The resonant dip corresponds to the polaron peak in the quasi-particle spectrum and its position reveals a small concentration-dependent energy shift, which we attribute to mediated interactions. We analyse the signal by applying a heuristic fit model (Methods), from which we extract the polaron energy peak position, which we identify with $\epsilon_\downarrow$. From the fits, we also extract the maximum transferred fraction of impurities from $K|0\rangle$ to $K|1\rangle$, $\mathcal{T}_{max}$. Based on experimental observables, we introduce the effective impurity concentration in the interacting state as $\tilde{\mathcal{C}} = \mathcal{C}_{K|0\rangle} \times \frac{1}{2}\mathcal{T}_{max}$, where $\mathcal{C}_{K|0\rangle} = \bar{n}_{K|0\rangle}/\bar{n}_{Li}$ is the concentration of the non-interacting $K|0\rangle$ atoms, given by the number density ratio of the two species. The factor $\frac{1}{2}$ in our definition of $\tilde{\mathcal{C}}$ arises from averaging the number of impurities, which are gradually injected from 0 to the final value during the RF pulse[21].

In the second step of our data analysis, we consider the dependence of the polaron energy $\epsilon_\downarrow$ on the impurity concentration $\tilde{\mathcal{C}}$ for fixed values of X. In Fig. 2b, we present an example of the corresponding procedure for the FB mixture, considering $X \approx 1$. The orange diamond and blue square represent the polaron energy extracted from the spectra shown in Fig. 2a, where $\tilde{\mathcal{C}} \approx 0.04$ and $\tilde{\mathcal{C}} \approx 0.16$, respectively. We assume a linear dependence to fit the observed behaviour (Fig. 2b, black line). From the obtained line, we can extract the mediated interaction coefficient $\bar{f}n_\downarrow/\epsilon_F$ from the slope, and the normalized single-impurity polaron energy $\epsilon_\downarrow^0/\epsilon_F$ from extrapolation to zero. In Fig. 2c, we present the measured polaron energies and the corresponding fits of the concentration dependence for different X values for the FB case.

For fermionic ^{40}K impurities (FF mixture), we proceed in essentially the same way, apart from details in the preparation process and a generally more noisy signal (Methods). The experimental conditions for the RF spectroscopic measurements stay close to the case of bosonic ^{41}K impurities (FB mixture), and the data analysis protocol is identical. Extended Data Fig. 1 is the analogue of Fig. 2 for the FF case. For all our recorded data, the concentration dependence of the polaron energy is consistent with a linear behaviour, as expected from equation (3), at every interaction strength for both FB and FF cases (Fig. 2 and Extended Data Fig. 1).

We can now compare our experimental results with the theoretical prediction of equation (3). As an important benchmark, we first confront the zero-concentration result $\epsilon_\downarrow^0$, as obtained from our linear fits, with the first term in equation (3). This comparison is reported in Fig. 3, demonstrating excellent agreement between the experimental results and polaron theory[12,17] in the whole range of interaction strengths explored in our experiment. Minor deviations observed for fermionic impurities for $X \gtrsim 1$ can be explained considering the finite temperature of our samples (Supplementary Section I). The overall agreement with a well-established limiting case represents a validity check for our measurements, particularly for the assumed linear dependence of $\epsilon_\downarrow$ on $\tilde{\mathcal{C}}$. The impurity quantum statistics cannot play a role in the single-impurity limit, which is in accordance with our experimental observations.

Let us now turn our attention to the main quantity of interest. In our linear fits, the slope yields the mediated interaction coefficient $\bar{f}n_\uparrow/\epsilon_F$. Most importantly, the experimental results displayed in Fig. 4 for the regime of weak-to-moderate interactions ($|X| \gtrsim 1$) clearly show the expected behaviour. For bosonic impurities, the downshift with increasing concentration reveals attraction ($\bar{f} < 0$) on both sides of resonance. In contrast, for fermionic impurities, the observed interaction between the polarons is repulsive ($\bar{f} > 0$) on both sides of resonance. Our observations, thus, highlight the essential difference between bosonic and fermionic impurities, which is the opposite sign of the mediated polaron–polaron interaction shift. Moreover, the observed strength of the mediated polaron–polaron interaction agrees—in the regime of weak and moderate interactions—with the static Fermi-liquid result for $\bar{f}$ given by equation (2).

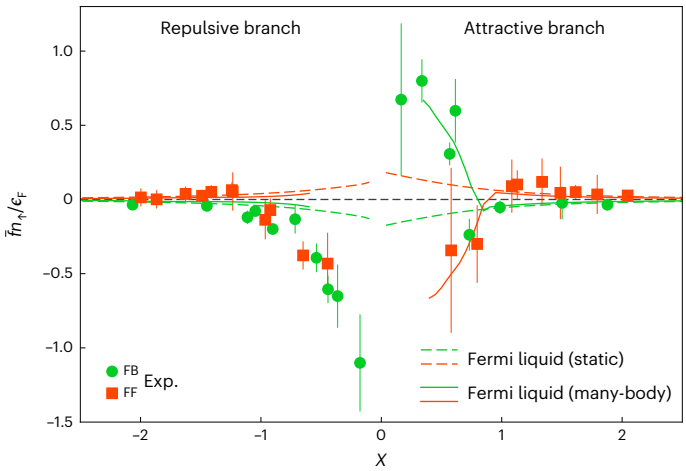

Fig. 5 | Mediated interaction coefficient across the resonance. The experimental results for $\bar{f}n_\uparrow/\epsilon_F$ for the FB (green circles) and FF (red squares) mixtures are compared with the static Fermi-liquid theory of equation (2) (dashed green and red lines for FB and FF, respectively) and with the corresponding microscopic many-body result (Supplementary Section II), assuming a density of dressed molecules equal to 2.5 times that of the impurities (solid green and red lines for FB and FF, respectively). The plot refers to the repulsive and attractive branches for negative and positive values of X, respectively. The error bars on $\bar{f}n_\uparrow/\epsilon_F$ correspond to the uncertainties of the linear fit and the errors on the Fermi energy. The error bars on X, smaller than the symbol size, represent the standard errors for each set of measurements.

In Fig. 5, we report the observed dependence of the mediated interaction coefficient across the full resonance, particularly exploring the strongly interacting regime of $-1 \lesssim X \lesssim 1$. For strong interactions, we observe striking deviations from the prediction of equation (2), both regarding the magnitude and sign of $\bar{f}$. On the attractive side of resonance ($X > 0$), a remarkable sign change of $\bar{f}$ is observed for both bosonic and fermionic impurities for $X \lesssim 1$; therefore, the interaction becomes repulsive or attractive, respectively. When the resonance is approached from the repulsive side ($X < 0$), the energy shift becomes negative corresponding to large and negative values of $\bar{f}$. This appears independent of the impurity quantum statistics, in contrast to the observations for moderate interaction strength and for the attractive side.

The solid lines in Fig. 5 show the prediction of a microscopic many-body calculation based on the ladder approximation generalized to non-zero impurity concentrations (Supplementary Section II). When expanded to the linear order in the impurity density, this naturally yields equation (1) for the polaron energy together with a microscopic expression for the interaction $f_{\mathbf{k},\mathbf{k}'}$ (refs. 29,30). This theory recovers equation (2) for weak impurity–medium interaction and low momenta, and generalizes this perturbative result by including strong two-body correlations and the momentum dependence of the interaction, thermal distribution of polarons, retardation and the presence of dressed molecules. We see that it recovers the experimental results on the attractive side ($X > 0$) including the observed sign change in the strong-coupling regime. The theory attributes this sign change to a non negligible thermal population of dressed molecules as their energy approaches that of the polaron close to resonance[18,31,32]. This can be understood from the fact that the coupling to higher-energy dressed molecules gives rise to a negative energy shift of the polarons[29]. For fermionic impurities, these dressed molecules are bosons and it follows that a thermal population will lead to Bose stimulation increasing this negative energy shift. This corresponds to an attractive polaron–molecule interaction that counteracts the repulsive polaron–polaron interaction for fermionic impurities, giving the observed decrease in the polaron energy for the FF mixture at a strong coupling. An analogous argument yields a repulsive polaron–molecule interaction for bosonic impurities, resulting in the abrupt increase in the calculated polaron energy in the FB mixture (Fig. 5). To calculate the many-body curves (Fig. 5), we have assumed a dressed molecule density 2.5 times the polaron density. This is consistent with the experimental conditions since a finite RF pulse width, along with a non-zero impurity concentration and temperature, smoothen the polaron–molecule transition and can give rise to similar dressed molecule concentrations in the cross-over regime[33]. We have restricted the plot range to the regions where the polaron residue exceeds 0.5.

The pronounced decrease in the energy of repulsive polarons in the strongly interacting regime ($-1 \lesssim X < 0$), which is independent of the impurity statistics, cannot be explained by our theory. We speculate that this may be due to a breakdown of the quasi-particle picture for a strong coupling. Indeed, the quasi-particle residue is small for strong coupling and the repulsive polaron becomes strongly damped[28], raising questions on a description in terms of quasi-particles. Our results, therefore, motivate further studies exploring the intricate interaction physics in the strongly interacting regime, which may involve intriguing physics well beyond the Fermi-liquid paradigm. Moreover, it would be interesting to further explore the breakdown of the quasi-particle picture with increasing concentration. Indeed, the underlying physics changes for $\mathcal{C} \approx 1$ to nearly balanced FB[34–37] and FF[38–40] mixtures; for $\mathcal{C} \gg 1$, the roles of the impurities and the medium are reversed[21].

Online content

Any methods, additional references, Nature Portfolio reporting summaries, source data, extended data, supplementary information, acknowledgements, peer review information; details of author contributions and competing interests; and statements of data and code availability are available at https://doi.org/10.1038/s41567-023-02248-4.

References

1. Noziéres, P. *Theory of Interacting Fermi Systems* (Benjamin, 1964).
2. Baym, G. & Pethick, C. *Landau Fermi-Liquid Theory* (Wiley-VCH, 2004).
3. Schirotzek, A., Wu, C.-H., Sommer, A. & Zwierlein, M. W. Observation of Fermi polarons in a tunable Fermi liquid of ultracold atoms. *Phys. Rev. Lett.* **102**, 230402 (2009).
4. Kohstall, C. et al. Metastability and coherence of repulsive polarons in a strongly interacting Fermi mixture. *Nature* **485**, 615–618 (2012).
5. Hu, M.-G. et al. Bose polarons in the strongly interacting regime. *Phys. Rev. Lett.* **117**, 055301 (2016).
6. Jørgensen, N. B. et al. Observation of attractive and repulsive polarons in a Bose-Einstein condensate. *Phys. Rev. Lett.* **117**, 055302 (2016).
7. Scazza, F. et al. Repulsive Fermi polarons in a resonant mixture of ultracold ^{6}Li atoms. *Phys. Rev. Lett.* **118**, 083602 (2017).
8. DeSalvo, B. J., Patel, K., Cai, G. & Cheng, C. Observation of fermion-mediated interactions between bosonic atoms. *Nature* **568**, 61–64 (2019).
9. Cetina, M. et al. Ultrafast many-body interferometry of impurities coupled to a Fermi sea. *Science* **354**, 96–99 (2016).
10. Muir, J. B. et al. Interactions between Fermi polarons in monolayer WS_2. *Nat. Commun.* **13**, 6164 (2022).
11. Tan, L. B. et al. Bose polaron interactions in a cavity-coupled monolayer semiconductor. *Phys. Rev. X* **13**, 031036 (2023).
12. Chevy, F. Universal phase diagram of a strongly interacting Fermi gas with unbalanced spin populations. *Phys. Rev. A* **74**, 063628 (2006).

13. Lobo, C., Recati, A., Giorgini, S. & Stringari, S. Normal state of a polarized Fermi gas at unitarity. *Phys. Rev. Lett.* **97**, 200403 (2006).
14. Combescot, R., Recati, A., Lobo, C. & Chevy, F. Normal state of highly polarized Fermi gases: simple many-body approaches. *Phys. Rev. Lett.* **98**, 180402 (2007).
15. Combescot, R. & Giraud, S. Normal state of highly polarized Fermi gases: full many-body treatment. *Phys. Rev. Lett.* **101**, 050404 (2008).
16. Prokof'ev, N. & Svistunov, B. Fermi-polaron problem: diagrammatic Monte Carlo method for divergent sign-alternating series. *Phys. Rev. B* **77**, 020408 (2008).
17. Massignan, P. & Bruun, G. M. Repulsive polarons and itinerant ferromagnetism in strongly polarized Fermi gases. *Eur. Phys. J. D* **65**, 83–89 (2011).
18. Trefzger, C. & Castin, Y. Impurity in a Fermi sea on a narrow Feshbach resonance: a variational study of the polaronic and dimeronic branches. *Phys. Rev. A* **85**, 053612 (2012).
19. Schmidt, R. et al. Universal many-body response of heavy impurities coupled to a Fermi sea: a review of recent progress. *Rep. Prog. Phys.* **81**, 024401 (2018).
20. Yan, Z. et al. Boiling a unitary Fermi liquid. *Phys. Rev. Lett.* **122**, 093401 (2019).
21. Fritsche, I. et al. Stability and breakdown of Fermi polarons in a strongly interacting Fermi-Bose mixture. *Phys. Rev. A* **103**, 053314 (2021).
22. Mora, C. & Chevy, F. Normal phase of an imbalanced Fermi gas. *Phys. Rev. Lett.* **104**, 230402 (2010).
23. Yu, Z., Zöllner, S. & Pethick, C. J. Comment on 'normal phase of an imbalanced Fermi gas'. *Phys. Rev. Lett.* **105**, 188901 (2010).
24. Yu, Z. & Pethick, C. J. Induced interactions in dilute atomic gases and liquid helium mixtures. *Phys. Rev. A* **85**, 063616 (2012).
25. Massignan, P., Bruun, G. M. & Smith, H. Viscous relaxation and collective oscillations in a trapped Fermi gas near the unitarity limit. *Phys. Rev. A* **71**, 033607 (2005).
26. Giraud, S. & Combescot, R. Interaction between polarons and analogous effects in polarized Fermi gases. *Phys. Rev. A* **85**, 013605 (2012).
27. Chin, C., Grimm, R., Julienne, P. S. & Tiesinga, E. Feshbach resonances in ultracold gases. *Rev. Mod. Phys.* **82**, 1225–1286 (2010).
28. Massignan, P., Zaccanti, M. & Bruun, G. M. Polarons, dressed molecules and itinerant ferromagnetism in ultracold Fermi gases. *Rep. Prog. Phys.* **77**, 034401 (2014).
29. Bastarrachea-Magnani, M. A., Camacho-Guardian, A. & Bruun, G. M. Attractive and repulsive exciton-polariton interactions mediated by an electron gas. *Phys. Rev. Lett.* **126**, 127405 (2021).
30. Bastarrachea-Magnani, M. A., Thomsen, J., Camacho-Guardian, A. & Bruun, G. M. Polaritons in an electron gas—quasiparticles and Landau effective interactions. *Atoms* **9**, 81 (2021).
31. Punk, M., Dumitrescu, P. T. & Zwerger, W. Polaron-to-molecule transition in a strongly imbalanced Fermi gas. *Phys. Rev. A* **80**, 053605 (2009).
32. Massignan, P. Polarons and dressed molecules near narrow Feshbach resonances. *Europhys. Lett.* **98**, 10012 (2012).
33. Ness, G. et al. Observation of a smooth polaron-molecule transition in a degenerate Fermi gas. *Phys. Rev. X* **10**, 041019 (2020).
34. Fratini, E. & Pieri, P. Pairing and condensation in a resonant Bose-Fermi mixture. *Phys. Rev. A* **81**, 051605 (2010).
35. Ludwig, D., Floerchinger, S., Moroz, S. & Wetterich, C. Quantum phase transition in Bose-Fermi mixtures. *Phys. Rev. A* **84**, 033629 (2011).
36. Yu, Z.-Q., Zhang, S. & Zhai, H. Stability condition of a strongly interacting boson-fermion mixture across an interspecies Feshbach resonance. *Phys. Rev. A* **83**, 041603 (2011).
37. Duda, M. et al. Transition from a polaronic condensate to a degenerate Fermi gas of heteronuclear molecules. *Nat. Phys.* **19**, 720–725 (2023).
38. Nascimbène, S. et al. Fermi-liquid behavior of the normal phase of a strongly interacting gas of cold atoms. *Phys. Rev. Lett.* **106**, 215303 (2011).
39. Gubbels, K. B. & Stoof, H. T. C. Imbalanced Fermi gases at unitarity. *Phys. Rep.* **525**, 255–313 (2013).
40. Pini, M., Pieri, P., Grimm, R. & Strinati, G. C. Beyond-mean-field description of a trapped unitary Fermi gas with mass and population imbalance. *Phys. Rev. A* **103**, 023314 (2021).

Methods

Spin states

For the RF spectroscopic measurements, the ^{6}Li atoms forming the spin-polarized FS are always kept in the lowest hyperfine spin state $(F, m_F) = (1/2, +1/2)$. In the preceding preparation process, two-component spin mixtures are exploited for evaporative cooling.

As the starting point for the measurements, the K atoms are prepared in an auxiliary state $\mathrm{K}|\mathrm{aux}\rangle$, which corresponds to the third-lowest spin state (1, +1) for ^{41}K and to the lowest state (9/2, −9/2) for ^{40}K. In our spectroscopic injection scheme, the initial state $\mathrm{K}|0\rangle$ is represented by the state (1, 0) for ^{41}K and by the state (9/2, −7/2) for ^{40}K. The final Feshbach-resonant state $\mathrm{K}|1\rangle$ corresponds to (1, +1) for ^{41}K and to (9/2, −5/2) for ^{40}K.

Sample preparation

The Li and K atoms are first loaded from a Zeeman-slowed atomic beam into a dual-species magneto-optical trap and then transferred into a single-beam optical dipole trap (ODT1), which is derived from a 200 W fibre laser at a wavelength of 1,070 nm. During the transfer process, we apply grey molasses cooling on the D1 line of Li, which reduces the temperature to about 50 μK and polarizes the majority of Li atoms into the lowest hyperfine spin state (1/2, +1/2) (refs. 41,42). Mixing the two lowest spin states with a resonant RF, we then produce a 50/50 mixture in the lowest two states (1/2, ±1/2). We hold the sample for a time of typically 0.5 s (3.0 s) in the FB (FF) case, in which spin relaxation induced by interspecies collisions polarizes the K atoms into the state $\mathrm{K}|\mathrm{aux}\rangle$ (refs. 43,44). This spin relaxation process is optimized at a magnetic field of ~200 G for ^{41}K and ~15 G for ^{40}K.

Evaporative cooling is implemented by ramping the power of ODT1 down to zero and ramping down the power of a crossed optical dipole trap (ODT2), which is turned on at the maximum power together with ODT1 at the loading stage. The ramp is performed in ~5 s and a wait time of 1 s is added to reach thermal equilibrium between the two species. During the evaporation stage, the K atom is sympathetically cooled by the Li atoms, which are in a mixture of (1/2, 1/2) and (3/2, −3/2) states at 485 G for the FB case and in a mixture of (1/2, 1/2) and (1/2, −1/2) states at 923 G for the FF case. The final power of ODT2 is adjustable to reach the desired temperature of the atomic clouds and we increase it in the final stage of the preparation process to reach the same trapping frequencies for each experimental run, minimizing the effect of optical shifts of the FR induced by the trapped light (see the supplementary information of ref. 45). The geometrically averaged trap frequencies are 117 Hz for ^{41}K and 193 Hz for Li for the FB mixture, and 158 Hz for ^{40}K and 271 Hz for Li for the FF mixture. ODT2 features an aspect ratio of about seven, with the weak axis oriented horizontally. The differential gravitational sag of both species amounts to about 3 μm and can be neglected since the FS is much larger than the K cloud.

After evaporative cooling, to obtain a fully polarized sample of Li in the (1/2, +1/2) state, we remove the atoms in the second spin state of Li by applying a resonant 10 μs light pulse at 567 G (1,180 G) in the FB (FF) case.

Then, the magnetic field is ramped close to the FR of interest near 335 G for the FB mixture and 155 G for the FF mixture. At this point, we switch to a different set of coils, which facilitates precise magnetic-field control to the level below a few milligauss. The trap contains a thermalized sample of roughly 10^5 Li atoms in the lowest hyperfine spin state and 10^4 $\mathrm{K}|\mathrm{aux}\rangle$ atoms. The temperature T is 102–137 nK in the FB case and 190–285 nK in the FF case. At these temperatures, the FS is deeply degenerate with $T/T_\mathrm{F} \approx 0.15$ and $T/T_\mathrm{F} \approx 0.25$ for the FB and FF mixtures, respectively. In contrast, the K impurities remain in the thermal regime.

To vary the impurity concentration in the initial spectroscopy state, we transfer the desired amount of atoms from the auxiliary state $\mathrm{K}|\mathrm{aux}\rangle$ to $\mathrm{K}|0\rangle$ using an RF pulse. In this way, keeping the total number of K atoms constant in the cooling process, we ensure identical starting conditions for measurements with variable impurity concentrations.

Detection

After the RF pulse that is used for probing the polaron spectrum, we switch off ODT2 and let the atomic cloud expand for a typical time of 1 ms and we detect the atoms by using state-selective absorption imaging. In the case of the FB mixture, we can directly image $\mathrm{K}|0\rangle$ and $\mathrm{K}|1\rangle$, using nearly closed optical transitions. In the FF case, however, because of the larger hyperfine structure of ^{40}K in combination with the lower magnetic field, optical transitions for the detection of $\mathrm{K}|0\rangle$ and $\mathrm{K}|1\rangle$ are leaky, which compromises the signal-to-noise ratio. Here we apply a resonant light pulse to remove $\mathrm{K}|1\rangle$ in 10 μs and apply a 96 μs RF π-pulse transferring atoms from $\mathrm{K}|0\rangle$ to $\mathrm{K}|\mathrm{aux}\rangle$, which permits imaging via a closed optical transition. In this way, we derive our spectroscopic signal from atoms remaining in state $\mathrm{K}|0\rangle$. For the FB case, to facilitate a direct comparison, we also define the corresponding spectroscopic signal based on atoms remaining in $\mathrm{K}|0\rangle$.

We determine the temperature of the mixture by a ballistic expansion of the thermal K cloud after releasing it from the trap, for both FB and FF cases. The Fermi energy of the Li cloud and the concentration of the non-interacting impurities are obtained from separate measurements in which we record the distributions of the Li and K atoms with the same initial conditions as in the polaron spectrum acquisition. These measurements are performed before each polaron spectrum is taken.

Effective quantities

To take into account spatial inhomogeneities in our harmonically trapped mixture, we introduce effective quantities defined by averaging over the spatial extent of the K cloud, as in previous works[9,21]. We introduce the K-averaged atom number densities, $\bar{n}_\mathrm{Li}$ and $\bar{n}_\mathrm{K}$, for both species, namely,

$$\bar{n}_{\mathrm{Li,K}} = \frac{1}{N_\mathrm{K}} \int n_{\mathrm{Li,K}}(\mathbf{r}) n_\mathrm{K}(\mathbf{r}) \mathrm{d}^3\mathbf{r}, \tag{4}$$

where $n_{\mathrm{Li,K}}(\mathbf{r})$ is the corresponding local number density of Li and K at position $\mathbf{r}$, respectively. Similarly, we define the effective Fermi energy as

$$\epsilon_\mathrm{F} = \frac{1}{N_\mathrm{K}} \int E_\mathrm{F}(\mathbf{r}) n_\mathrm{K}(\mathbf{r}) \mathrm{d}^3\mathbf{r}, \tag{5}$$

where the local Fermi energy at position $\mathbf{r}$ is given by

$$E_\mathrm{F}(\mathbf{r}) = \frac{\hbar^2 (6\pi^2 n_\mathrm{Li}(\mathbf{r}))^{2/3}}{2m_\mathrm{Li}}. \tag{6}$$

From this, we define the effective Fermi wave number as $k_\mathrm{F} = \sqrt{2m_\mathrm{Li}\epsilon_\mathrm{F}}/\hbar$ (ref. 4). We emphasize that owing to the much smaller size of the K cloud, the effect of inhomogeneity in n_Li, and thus in E_F, is small. For n_Li, this amounts to about 10%.

Control of interactions

The s-wave interaction of bosonic or fermionic impurity atoms in the spectroscopy state $\mathrm{K}|1\rangle$ with the ^{6}Li atoms forming the FS can be controlled by means of interspecies FRs. The s-wave scattering length follows the standard expression

$$a(B) = a_\mathrm{bg}\left(1 - \frac{\Delta}{B - B_0}\right), \tag{7}$$

where B_0 represents the resonance centre, Δ denotes the magnetic width and a_bg is the background scattering length.

For the ^{41}K–^{6}Li resonance (FB case), the relevant parameter values are as follows[21,46]: $B_0 = 335.080(1)$ G, $\Delta = 0.9487$ G and $a_\mathrm{bg} = 60.865 a_0$.

The closed-channel-dominated resonance[27] is further characterized by a differential magnetic moment $\delta\mu/h = 2.660(8)$ MHz G^{-1}. For the range parameter, as introduced elsewhere[47], this corresponds to the value $R^* = 2{,}241(7)a_0$ or, if expressed in relation to the Fermi wave number in a dimensionless way, to $k_F R^* = 0.54$.

For the ^{40}K–^{6}Li resonance (FF case), the relevant parameter values are as follows[9,48]: $B_0 = 154.7126(5)$ G, $\Delta = 0.88$ G and $a_{bg} = 63.0a_0$. The resonance is further characterized by a differential magnetic moment $\delta\mu/h = 2.3$ MHz G^{-1}. For the range parameter, this corresponds to $R^* = 2{,}405(63)a_0$ or $k_F R^* = 0.62$. Here the reported values of B_0 and R^* are determined during the preparation of the experiment reported in this work, following the molecule dissociation technique described elsewhere[21].

We emphasize the very similar character of the resonances in the FB and FF cases. Although they are both closed-channel dominated[27], their width is large enough to stay in a near-universal interaction regime ($k_F R^* < 1$) with the FS.

For both K isotopes in the initial spectroscopy state K|0⟩ and the auxiliary state K|aux⟩, the interaction with the FS remains weak with scattering lengths of about $60a_0$ (ref. 48). This is just enough for thermalization with the medium in the sympathetic cooling process, but for the spectroscopic scheme, this background interaction is fully negligible.

We further note that the weak intraspecies interactions between all the considered K spin states (K|0⟩, K|aux⟩ and K|1⟩) are characterized by small scattering lengths, of the order of $60a_0$ and $170a_0$ for the FB[49] and FF[50] mixtures, respectively. In addition, spin-polarized fermionic K atoms do not interact with each other in the s wave due to Pauli exclusion.

Spectroscopic signal and fit

Our choice of the number $N_{K|0\rangle}$ of atoms remaining in K|0⟩ after the RF pulse as the spectroscopic observable has the advantage of working equally well for the FB and FF cases. In previous work, we had chosen $N_{K|1\rangle}/N_{K_{tot}}$ (number of atoms in K|1⟩ after the pulse divided by the total atom number)[4,21] or $(N_{K|1\rangle} - N_{K|0\rangle})/N_{K_{tot}}$ (ref. 9) to extract the signal. However, the absence of a sufficiently closed optical transition impedes an efficient detection of atoms in K|1⟩, particularly for the FF mixture. Moreover, possible losses in the transfer process may complicate the interpretation of a signal based on $N_{K|1\rangle}$.

We take measurements in a range of about ±35 mG around the FR centre. This implies that we need knowledge of our magnetic field on the level of a milligauss. The main limitation in our system is given by slow drifts in the magnetic field during the measurements. To deal with this drift, we perform magnetic-field calibration measurements before and after each spectrum is recorded and we reject the spectra for which the difference in the results of these two measurements is larger than 2 mG (1 mG) for FB (FF). Moreover, we perform the measurements in the shortest time possible and, as a consequence, we sample the quasi-particle spectrum in a region centred around the polaron peak (typically less than ϵ_F wide), not recording the full background.

As a well-established fact, the spectroscopy signal has two components: one due to the polaron and one due to the presence of an underlying incoherent background[9,21,28]. In previous work[4,21], the broad background was approximated by a Gaussian, so that the complete polaron spectrum could be modelled by a double-Gaussian function. Given the incompleteness of the recorded background in the present measurements, applying a double-Gaussian fit to our spectrum is not possible. To circumvent this, we fit with a Gaussian combined with a linear background, the latter mimicking the presence of the non-fully recorded incoherent background, especially present in the strongly interacting regime and negligible for weak interactions. We checked that fitting the selected spectra taken over a wider range with a Gaussian and a linear fit and with a double Gaussian leads to values of the polaron energy that are in each other's error bars (Extended Data Fig. 2).

Theory

To describe strong-coupling effects including the momentum dependence of the effective interaction, a thermal distribution of polarons, retardation and the presence of dressed molecules, we apply the microscopic many-body theory. In this approach, the polaron energy is given by solving

$$\epsilon_{\mathbf{k}\downarrow} = \hbar^2 k^2/2m_\downarrow + \Sigma(\mathbf{k}, \epsilon_{\mathbf{k}\downarrow}), \tag{8}$$

where $\Sigma(\mathbf{k}, \omega)$ is the impurity self-energy. To connect this to the Landau form given by equation (1), we expand the self-energy to a linear order in the impurity population, writing $\Sigma(\mathbf{k}, \omega) \simeq \Sigma^0(\mathbf{k}, \omega) + \sum_{\mathbf{k}'} n_{\mathbf{k}'\downarrow} \partial_{n_{\mathbf{k}'\downarrow}} \Sigma(\mathbf{k}, \omega)|_{n_{\mathbf{k}'\downarrow}=0}$, where $\Sigma_0(\mathbf{k}, \omega)$ denotes its value for a single impurity. Solving equation (8) to the linear order in the impurity population then yields equation (1) with the interaction

$$f_{\mathbf{k},\mathbf{k}'} = Z_{\mathbf{k}} \left. \frac{\partial \Sigma(\mathbf{k}, \epsilon_{\mathbf{k}\downarrow})}{\partial n_{\mathbf{k}'\downarrow}} \right|_{n_{\mathbf{k}'\downarrow}=0}, \tag{9}$$

where $Z_{\mathbf{k}} = [1 - \partial_\omega \Sigma^0(\mathbf{k}, \omega)_{\omega=\epsilon_{\mathbf{k}\downarrow}}]^{-1}$ is the quasi-particle residue. Equation (9) shows, in general, how the effective interaction between quasi-particles can be calculated from the microscopic many-body theory.

To proceed, we calculate the self-energy using the ladder approximation, which is remarkably accurate for describing isolated Fermi polarons even for a strong interaction[28]. To compute the polaron–polaron coupling at vanishing temperature and momentum f_0 introduced in equation (2), one only needs the single-impurity self-energy, since $\Delta N = -Z\partial_{\epsilon_F} \Sigma^0(0, \epsilon^0_{0\downarrow})$. The evaluation of the general coupling $f_{\mathbf{k},\mathbf{k}'}$ obtained in equation (9) instead requires that the self-energy is computed for a non-zero impurity concentration (Supplementary Section II). This yields an extra term in the self-energy coming from the interaction of the polaron with dressed molecules, which becomes non negligible close to resonance where the dressed molecule energy approaches that of the polaron. The theory predicts the interaction between dressed molecules and polarons to be attractive/repulsive for fermionic/bosonic impurities[29].

Data availability

Experimental and theoretical data displayed in the figures of this Article are available via Figshare at https://doi.org/10.6084/m9.figshare.23633919 (ref. 51). Source data are provided with this paper.

Code availability

The theoretical codes are available from P.M. (pietro.massignan@upc.edu) and M.A.B.-M. (bastarrachea@xanum.uam.mx) upon request.

References

41. Burchianti, A. et al. Efficient all-optical production of large ^{6}Li quantum gases using D_1 gray-molasses cooling. *Phys. Rev. A* **90**, 043408 (2014).
42. Fritsche, I. *Sub-Doppler Cooling of Fermionic Lithium*. Master's thesis, Univ. of Innsbruck (2015).
43. Spiegelhalder, F. M. et al. All-optical production of a degenerate mixture of ^{6}Li and ^{40}K and creation of heteronuclear molecules. *Phys. Rev. A* **81**, 043637 (2010).
44. Lous, R. S., Fritsche, I., Jag, M., Huang, B. & Grimm, R. Thermometry of a deeply degenerate Fermi gas with a Bose-Einstein condensate. *Phys. Rev. A* **95**, 053627 (2017).
45. Cetina, M. et al. Decoherence of impurities in a Fermi sea of ultracold atoms. *Phys. Rev. Lett.* **115**, 135302 (2015).

46. Lous, R. S. et al. Probing the interface of a phase-separated state in a repulsive Bose-Fermi mixture. *Phys. Rev. Lett.* **120**, 243403 (2018).
47. Petrov, D. S. Three-boson problem near a narrow Feshbach resonance. *Phys. Rev. Lett.* **93**, 143201 (2004).
48. Naik, D. et al. Feshbach resonances in the ^{6}Li-^{40}K Fermi-Fermi mixture: elastic versus inelastic interactions. *Eur. Phys. J. D* **65**, 55–65 (2011).
49. Lysebo, M. & Veseth, L. Feshbach resonances and transition rates for cold homonuclear collisions between ^{39}K and ^{41}K atoms. *Phys. Rev. A* **81**, 032702 (2010).
50. Ludewig, A. *Feshbach Resonances in ^{40}K*. PhD thesis, Univ. of Amsterdam (2012).
51. Baroni, C., Bastarrachea-Magnani, M. A. et al. Mediated interactions between Fermi polarons and the role of impurity quantum statistics. figshare. Dataset. https://doi.org/10.6084/m9.figshare.23633919 (2023).

Acknowledgements

We acknowledge stimulating discussions with J. Dalibard, M. Parish, J. Levinsen and Z. Wu. The project has received partial funding from the European Research Council (ERC) under the European Union's Horizon 2020 research and innovation programme (grant agreement no. 101020438—SuperCoolMix). P.M. acknowledges support by grant PID2020-113565GB-C21 from MCIN/AEI/10.13039/501100011033, by grant 2021 SGR 01411 from the Generalitat de Catalunya and by the ICREA Academia program. G.M.B. acknowledges support from the Danish National Research Foundation through the Center of Excellence 'CCQ' (grant agreement no. DNRF156).

Author contributions

C.B. conceived and carried out the experiment and analysed the data. B.H., I.F. and E.D. performed additional measurements supporting the experiment. G.A. and E.K. provided support for the operation of the setup. R.G. directed the experiment. M.A.B.-M., P.M. and G.M.B. provided theoretical guidance and developed the theoretical model. C.B., R.G., M.A.B.-M., P.M. and G.M.B. wrote the manuscript. All authors contributed to the discussion and the interpretation of the results.

Competing interests

The authors declare no competing interests.

Additional information

Extended data is available for this paper at https://doi.org/10.1038/s41567-023-02248-4.

Supplementary information The online version contains supplementary material available at https://doi.org/10.1038/s41567-023-02248-4.

Correspondence and requests for materials should be addressed to Cosetta Baroni.

Peer review information *Nature Physics* thanks Ariel Sommer and the other, anonymous, reviewer(s) for their contribution to the peer review of this work.

https://doi.org/10.1038/s41567-023-02248-4

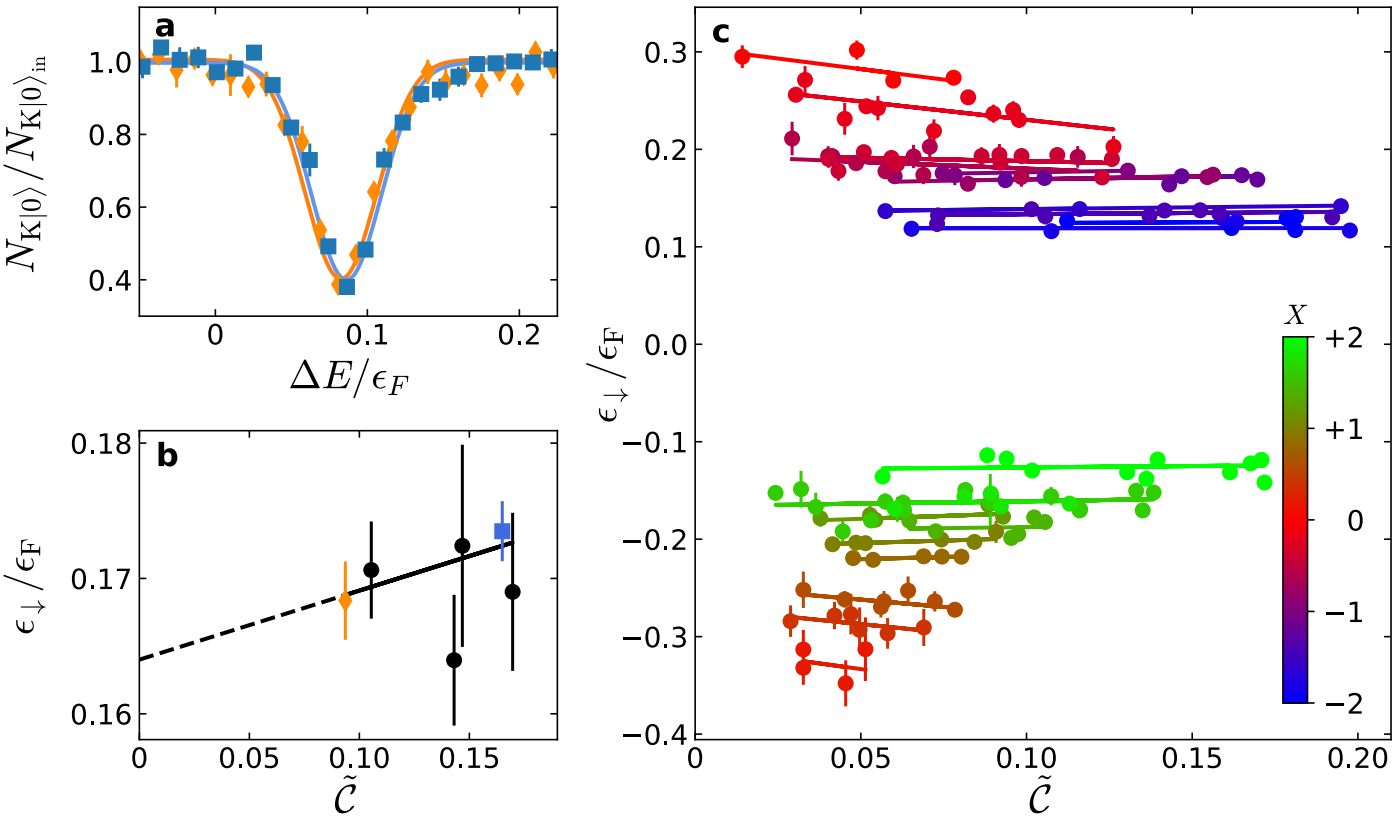

Extended Data Fig. 1 | Dependence of the polaron energy on the impurity concentration. For the FF case, the main steps of measurements and data analysis are illustrated. **a**, Two exemplary spectroscopy signals (normalized to the initial atom number) taken at $X = -1.41$ for different values of the interacting impurity concentration (blue squares $\tilde{\mathcal{C}} = 0.17$, orange diamonds $\tilde{\mathcal{C}} = 0.09$). The solid lines are fits with a Gaussian function on a linear background (the latter being negligibly small in the present data). The error bars represent the standard errors from typically 5-6 measurement repetitions. **b**, Polaron energy as a function of impurity concentration for $X = -1.41$. The blue square and the orange diamond correspond to the exemplary spectra presented in panel **a**. The black line represents a linear fit to the data with the dashed line showing the extrapolation to zero density. **c**, Polaron energy as a function of impurity concentration for different values of the interaction parameter X. From center to top (blue to red) increasing repulsion, from center to bottom (green to red) increasing attraction. Statistical uncertainties for **b** and **c** are evaluated taking into account fit uncertainties from analyzing the spectra and errors on the Fermi energy.

https://doi.org/10.1038/s41567-023-02248-4

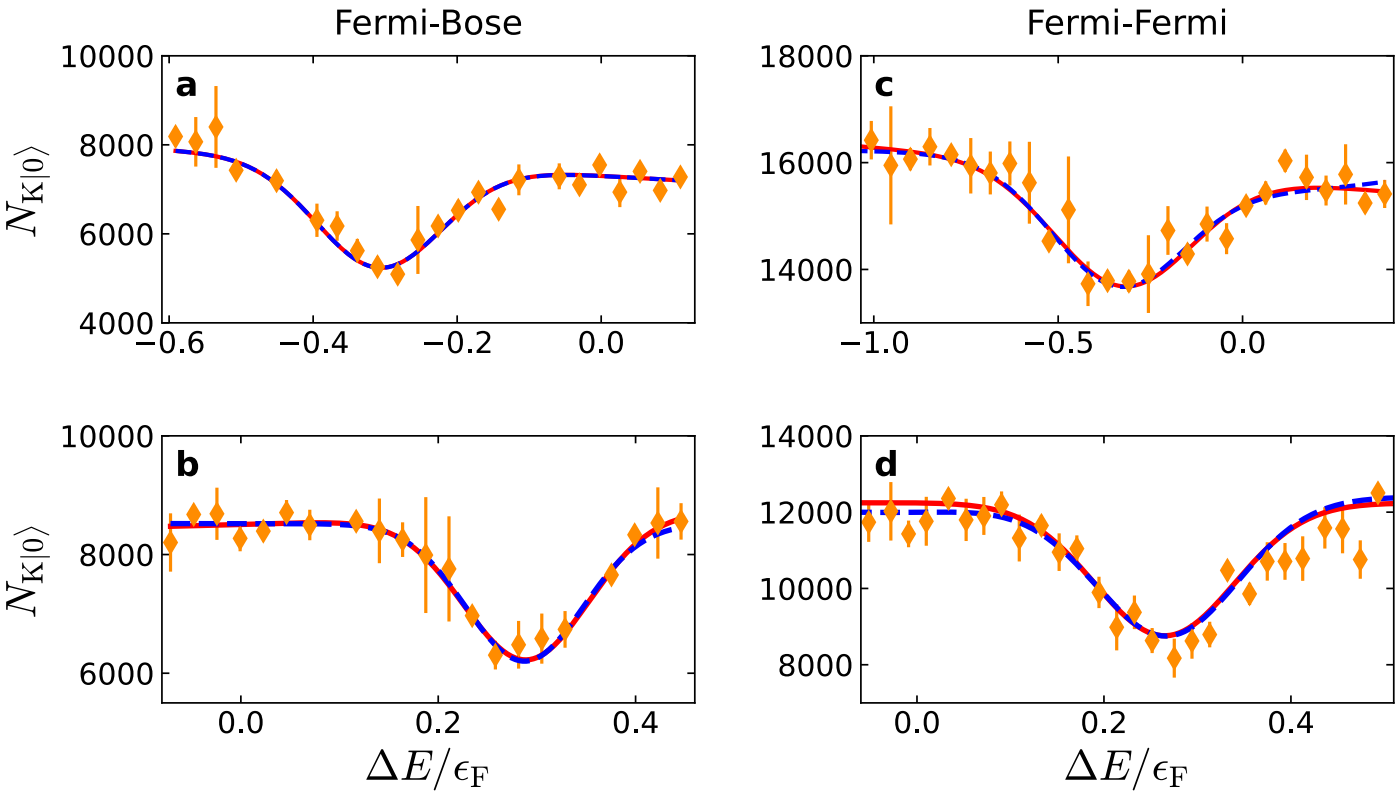

Extended Data Fig. 2 | Typical RF spectra in the strongly interacting regime and comparison between two fitting functions. Spectroscopy signals for the FB case with $X = 0.36$ and $\tilde{\mathcal{C}} = 0.07$ (**a**) and $X = -0.34$ and $\tilde{\mathcal{C}} = 0.07$ (**b**), and for the FF case with $X = 0.47$ and $\tilde{\mathcal{C}} = 0.03$ (**c**) and $X = -0.47$ and $\tilde{\mathcal{C}} = 0.08$ (**d**) The solid red lines are fits with a Gaussian function on a linear background, the dashed blue lines are fits with a double Gaussian. The error bars represent the standard errors from typically 5-6 measurement repetitions.